Nanometer-Sized Zeolite X Crystals: Use as Photochemical Hosts

Norma B. Castagnola and Prabir K. Dutta*

Department of Chemistry, The Ohio State University, 100 West 18th Ave., Columbus, Ohio 43210

Received: November 6, 1997; In Final Form: January 8, 1998

A patent procedure was followed to synthesize 250 nm aggregates of individual 13 ± 2.5 nm crystallites of zeolite X. A low-temperature aging step and addition of sucrose to the reaction mixture were required to get optimum quality of crystals. Conventional ship-in-a-bottle synthesis of $Ru(bpy)_3^{2+}$ in the cages of these nanocrystallites resulted in considerable framework degradation, with only 10% of the crystallinity in the original crystals being retained. The degradation occurred due to exposure to mild acidity and thermal treatment during synthesis of $Ru(bpy)_3^{2+}$. The procedure was modified to avoid acidity in the initial ion-exchange step of $Ru(NH_3)_6^{3+}$, resulting in a $Ru(bpy)_3^{2+}$−zeolite with 75% of the crystallinity retained. Acidity generated during conversion of $Ru(NH_3)_6^{3+}$ to $Ru(bpy)_3^{2+}$ was thought to be responsible for the degradation. A third procedure starting with the highly air-sensitive $Ru(NH_3)_6^{2+}$ resulted in formation of $Ru(bpy)_3^{2+}$−zeolite with about 90% crystallinity. In all three procedures, the $Ru(bpy)_3^{2+}$ molecules were entrapped within the framework. Ion exchange of viologen molecules and the fluorescence quenching of photoexcited $Ru(bpy)_3^{2+}$ by intrazeolitic viologen increased with the increase of zeolite crystallinity. Interfacial zeolite−solution electron transfer upon visible light photoexcitation of the $Ru(bpy)_3^{2+}$−zeolite−viologen system demonstrated an increase in permanent charge separation efficiency as the crystallinity of the zeolite is preserved. Because of the higher surface-to-volume ratios, the charge separation efficiency in the nanocrystallites was a factor of 2 better than conventional micron-sized zeolite Y crystallites under identical photolysis conditions.

Introduction

There has been considerable research over the past three decades in synthesis of large zeolite crystals, and the sizes are currently approaching the sub-millimeter range.[1] This interest is driven by possible technological applications of larger crystals and also because crystal structures can be better determined using diffraction methods. Less work has been done on zeolite crystals at the other extreme, i.e., crystals with sizes of the order of nanometers. Attempts to prepare smaller crystallites by grinding micron-sized crystals are not a viable method since considerable degradation of the structure occurs.[2] There have been several reports in the literature on direct synthesis of small zeolite crystallites, including zeolites A, Y, ZSM-5, zeolite L, silicalite, and 1-hydroxysodalite.[3] Applications of these nanocrystals in thin zeolite film formation and catalysis has been reported.[4]

Several reasons exist for pursuing the chemistry of small crystallites. First, with small enough crystals, transparent colloidal dispersions can be made. This would be of considerable advantage for carrying out various spectroscopic studies on zeolite-entrapped species. Second, there is increasing evidence that electrochemical measurements such as cyclic voltammetry sample the very surface layers of zeolites.[5] Thus, stronger electrochemical signals of entrapped complexes should be obtainable from smaller crystallites. Third, there is considerable interest in the development of zeolite supports for catalytic[6] and photochemical reactions,[7] and smaller crystallites could be of significant benefit.

Our interest is in examining the preparation and properties of small faujasite-type zeolite crystallites for artificial photosynthetic applications. This would require assembly of metal complexes inside the nanocrystallites, and to the best of our knowledge, no studies in this area have been reported. Synthesis of crystallites of zeolite Y with dimensions of 100 nm has appeared in the literature.[8] The patent literature reports crystallites even smaller (∼30 nm) for "faujasite" crystals[9] and is the focus of this study. We demonstrate here that these "faujasite" crystals are representative of zeolite X. Both zeolites X and Y possess the same framework but are differentiated based on the Si/Al ratios. Zeolite Y has a Si/Al ratio greater than 1.5, and zeolite X has a Si/Al ratio less than 1.5. We have synthesized $Ru(bpy)_3^{2+}$ inside the zeolite cages by a ship-in-a-bottle approach. Because of the poor acid and thermal stability of zeolite X, we had to modify the procedure for $Ru(bpy)_3^{2+}$ synthesis to maintain zeolite integrity. Photochemical charge separation of the $Ru(bpy)_3^{2+}$−viologen−nanocrystalline zeolite was examined. Charge separation efficiencies under identical photolysis conditions were a factor of 2 better for nanocrystalline X than with conventional micron-sized zeolite Y.

Experimental Section

A. Synthesis of Zeolite. The zeolite was synthesized from aqueous alkali metal silicate and aluminate solutions with a molar ratio of $SiO_2/Al_2O_3 \sim 6$ following a patent literature procedure.[9] The sodium silicate solution was prepared as follows: 78 mL of H_2O and 29.5 mL of aqueous NaOH (50%) solution were added to 96 g of sodium silicate solution (Sigma, 27% SiO_2 in 14% NaOH) with stirring, and the solution was chilled to <5 °C. The sodium aluminate solution was obtained by mixing 61 mL of H_2O and 25.5 mL of the NaOH (50%) solution with 18.3 g of $NaAlO_2 \cdot {}^3/_2H_2O$ (Chem Service), and the mixture was heated until clear and then chilled to <5 °C. Seventy-five grams of crushed ice was added to each solution. The silicate and aluminate solutions were immediately mixed in a Teflon bottle, and the mixture was set aside for 5 min. A gel formed. Then 12 g of sucrose is added to the gel, and the

S1089-5647(98)00103-5 CCC: $15.00
Published on Web 02/12/1998

mixture is aged with stirring under ambient conditions for 16 h. After aging, the solution was heated at 100 °C in an oil bath for 4 h with stirring. After the hydrothermal reaction, the solid was separated by centrifugation, washed several times with deionized water, and dried in air. Product yield was ~25 g.

B. Synthesis of $Ru(bpy)_3^{2+}$−Zeolite. Three methods were used for the intrazeolitic synthesis of $Ru(bpy)_3^{2+}$ inside the zeolite, the rationale for which is discussed later. In the first procedure, the zeolite was calcined at 500 °C overnight under a flow of oxygen. The Ru-entrapped complex was prepared by an extension of the method described by Lunsford and co-workers.[10] Two grams of calcined crystals of zeolite was ion-exchanged with 0.028 g of $Ru(NH_3)_6Cl_3$ (0.09 mmol, Strem Chemicals) in 120 mL of acidified H_2O (pH 5.2). After stirring for 1 h under N_2, the solid was filtered and dried in a vacuum oven. The $Ru(NH_3)_6^{3+}$−zeolite was then dry-mixed with 0.051 g of bipyridine (0.315 mmol, Aldrich), pressed into pellets, and transferred to a tube. The tube was evacuated at 10^{-4} Torr for 6 h, closed to vacuum, and heated at 200 °C for 24 h followed by evacuation for an additional 2 h. The product was washed twice with a 0.1 M NaCl solution to remove any surface species. The excess ligand was Soxhlet-extracted with methanol until bipyridine is no longer present in the solvent (typically 4 weeks) as measured by UV−visible spectroscopy. The second method was similar to the first, except that the zeolite was not calcined and $Ru(NH_3)_6^{3+}$ was ion-exchanged in a degassed aqueous suspension at 4 °C. In the third method, 60 mL of water containing 1 g of zeolite was purged with N_2 for 2 h. Under anaerobic conditions, 9 mg of $Ru(NH_3)_6Cl_2$ was added to the zeolite suspension, and the mixture was stirred under N_2 for 6 h. The filtered $Ru(NH_3)_6^{2+}$−zeolite was resuspended in a deaerated ethanolic solution containing 100 mg of bpy. The ethanol was evaporated, and the remaining solid was evacuated at 10^{-4} Torr for 6 h and then heated to 200 °C for 24 h. Similar treatment for purification as in the above procedures was done with the sample. The Ru complex loading was determined by X-ray fluorescence (Kevex 0700/7000).

C. Characterization. Sample integrity was monitored by X-ray powder diffraction. The XRD patterns were obtained with a Rigaku Geigerflex diffractometer using Ni-filtered Cu Kα radiation (40 kV and 35 mA). The crystal size was calculated from the peak broadening by Scherrer's equation using LaB_6 as a standard.[11] Particle morphology was obtained by a JEOL 820 scanning electron microscope. The IR spectra (samples diluted with KBr) were measured using a FTIR Mattson Cygnus 100 spectrophotometer. The Raman spectra were obtained by excitation at 488 nm (Spectra Physics argon ion laser, model 171) using a Spex 500M monochromator with a Princeton Instruments CCD detector (LN/CCD-1100PBU-VAR). A Shimadzu UV 265 spectrometer equipped with a Harrick diffuse reflectance attachment was used to obtain UV−vis spectra, using the zeolite X as background. ^{29}Si and ^{27}Al solid-state NMR spectra were recorded on a Bruker AM 500.

D. Viologens. *N,N′*-Tetramethylene-2,2′-bipyridinium dibromide (DQ^{2+}) was prepared as described by Homer and Tomlinson.[12a] Propyl viologen sulfonate (PVS) was also prepared following literature procedures.[12b] Methyl viologen (MV^{2+}) was purchased from Aldrich and recrystallized from methanol/acetone solvent.

E. Photolysis. The light source was a xenon arc lamp (model A1010, 150−200 W) equipped with a water filter, a 420 nm cutoff filter, and a mirror that reflects radiation in the range 420−650 nm. The power of the radiation incident on the sample was measured by a Coherent 210 power meter to be 250 mW/cm^2. Forty milligrams of $Ru(bpy)_3^{2+}$−zeolite was exchanged twice with a 0.1 M solution of the viologen for 24 h. Ten milligrams of the zeolite sample and 10 mg of PVS were placed in an NMR tube with a micro spinning bar and evacuated for 1 day at 10^{-5} Torr. Degassed water was distilled over and the suspension freeze−pump−thawed three times. The tube was sealed and photolyzed, and the growth of PVS radical in solution was monitored with a UV spectrophotometer.

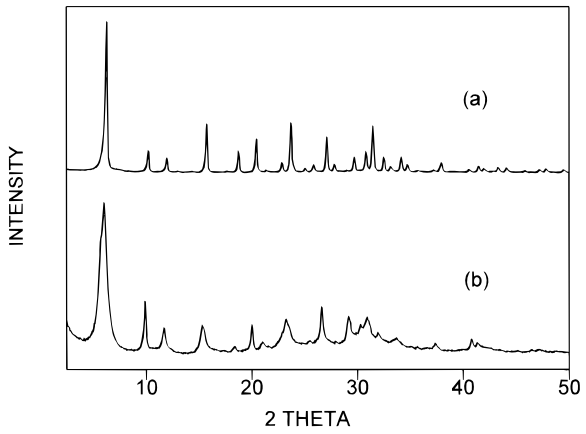

Figure 1. Powder diffraction patterns of (a) commercial zeolite Y and (b) nanocrystalline zeolite X.

Results and Discussion

A. Zeolite Synthesis and Characterization. The patent procedure we have followed for synthesis of small crystals[9] is similar to conventional faujasite synthesis, with two additional steps. First, the reactants are cold-mixed at 4 °C and gradually allowed to warm to room temperature, and second, sucrose is added to the reaction mixture during the aging step. Figure 1 compares the XRD powder patterns of crystals obtained by this procedure (Figure 1b) with commercial micron-sized zeolite Y (Figure 1a). It is immediately apparent that the diffraction lines are significantly broadened, indicating a smaller crystallite size. Experiments were repeated without sucrose as well as in the absence of the aging step. Faujasite crystals were obtained in both cases, though the crystallinity as determined by diffraction was considerably poorer than the process that involved both aging and addition of sucrose. The role of aging is well recognized in zeolite synthesis and helps in the nucleation process. It is unclear what role the sucrose is playing. It is known from the literature that sucrose will be hydrolyzed to lactic acid in the presence of base at high temperatures,[13] similar to the conditions reported here. Lactate ion is known to form weak complexes with Al^{3+}.[14] The presence of Al^{3+} chelating ligands will influence faujasite synthesis, as shown by Charnell[1] with triethanolamine as ligand and exploited in zeolite A and X synthesis by others.[15] Further research is needed to clarify the exact role played by sucrose. Nevertheless, it is clear from Figure 1 that small faujasite crystals are being made. Based on Scherrer's equation,[11] an average crystallite size of 13 ± 2.5 nm was calculated from the change in bandwidth of the powder diffraction peaks at 2θ of 6° (111), 16° (331), and 27° (642). Crystals recovered after 4 h of synthesis time are used in this study, since longer heating times produced crystals with a broader size distribution.

Figure 2 shows the scanning electron microscope image of the nanocrystalline zeolites. The particles are agglomerated, with sizes of these aggregates being 250 nm and composed of approximately 30 nm particles. The discrepancy between the microscopy and diffraction is not surprising considering the

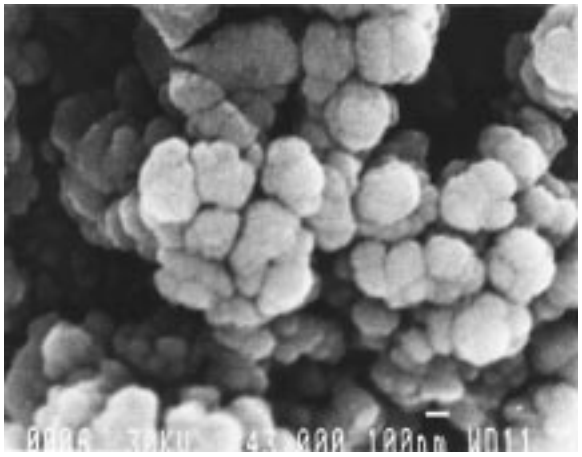

Figure 2. SEM micrograph of nanocrystalline zeolite X.

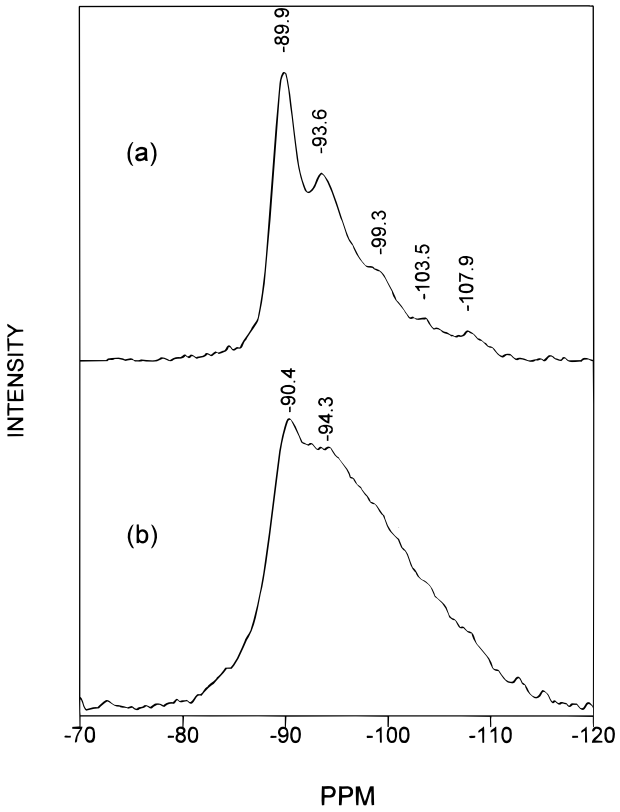

Figure 3. ^{29}Si NMR spectra of (a) as-synthesized nanocrystalline zeolite X and (b) after synthesis of $Ru(bpy)_3^{2+}-X(10)$.

difficulty of estimating size from SEM at the nanometer level. Since diffraction peak broadening is directly controlled by size, it provides a better estimate of the true size of these crystallites. Dispersion of the 250 nm aggregates into smaller crystallites was not possible by sonication.

Further characterization of these crystallites was done by ^{29}Si, ^{27}Al NMR, and vibrational spectroscopy. These data are shown in Figures 3−5. Figure 3a is the ^{29}Si NMR spectra of the as-synthesized product. The strongest resonance in the spectrum is characteristic of $Si(OAl)_4$ species.[16] By curve deconvolution into the various $Si(OAl)_n$ signals, we calculate the Si/Al ratio to be 1.3, suggesting that the crystallites are zeolite X. The ^{27}Al NMR in Figure 4a shows a single peak characteristic of Al in tetrahedral coordination. Figure 5a shows the infrared spectrum of the as-synthesized material. The peaks compare favorably well with previously published data on zeolite X.[17] The most prominent Raman band of these crystallites is observed

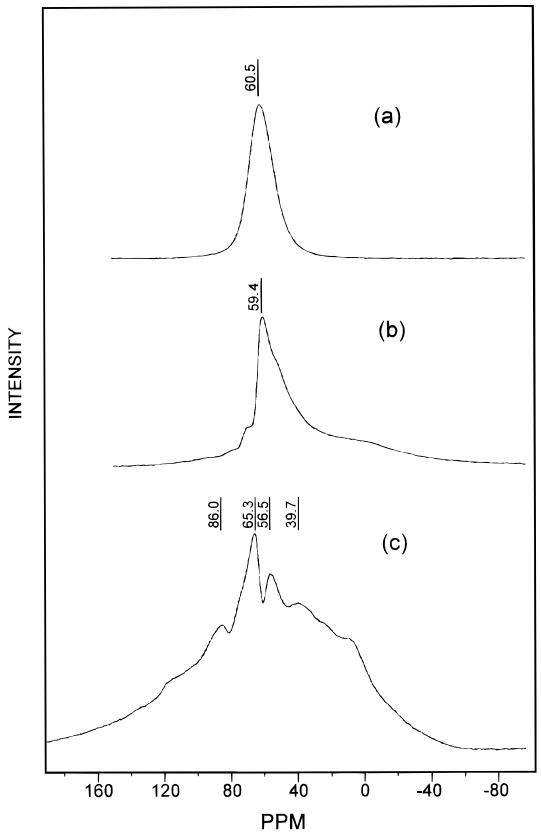

Figure 4. ^{27}Al NMR spectra of (a) as-synthesized nanocrystalline zeolite X, (b) after synthesis of $Ru(bpy)_3^{2+}-X(10)$, and (c) after exposure of nanocrystalline zeolite X to pH 5.2 and heating at 200 °C (no washing with NaCl).

at 503 cm^{-1} (not shown), whereas previous studies have shown that this band appears at 513 cm^{-1} for zeolite X.[18] Red shifts in frequency have been reported previously for GaAs, Si, and CeO_2 crystallites as a function of decreasing size.[19] This arises because in the smaller particles the momentum conservation is partially relaxed. Thus, infrared and NMR spectroscopies support the formation of zeolite X, and the Raman data suggest that the crystallites are small, in agreement with the microscopy and diffraction data.

B. Synthesis of Intrazeolitic $Ru(bpy)_3^{2+}$. *Method 1.* The conventional method of synthesis of $Ru(bpy)_3^{2+}$ involves ion exchange of $Ru(NH_3)_6^{3+}$ at pH 5 into a calcined zeolite followed by heating at 200 °C with bpy ligand for 24 h. With this procedure, the diffuse reflectance spectrum of $Ru(bpy)_3^{2+}$ formed in the zeolite was comparable with earlier studies on zeolite-encapsulated Ru complexes.[20] The sample was analyzed by X-ray fluorescence to contain 42 μmol of $Ru(bpy)_3^{2+}$ per gram of zeolite, or ∼1 complex per 12 supercages. However, the powder diffraction pattern (Figure 6b) exhibits a decrease in peak intensities (averaged over the following reflections: 111, 220, 311, 331, 440) corresponding to 10% of the original sample (Figure 6a), indicating framework degradation. Henceforth, we refer to this sample as $Ru(bpy)_3^{2+}-X(10)$. The $Ru(bpy)_3^{2+}$ was found to be firmly entrapped in the zeolite, and extensive ion exchange with 0.1 M NaCl did not displace any complex. Thus, the structural collapse of the framework occurs around the $Ru(bpy)_3^{2+}$ complex.

Spectroscopic studies on $Ru(bpy)_3^{2+}-X(10)$ provide evidence of the nature of the degradation. Figure 3b shows the solid-state ^{29}Si NMR, and Figure 4b shows the ^{27}Al NMR after synthesis of the $Ru(bpy)_3^{2+}$, which includes washing the sample

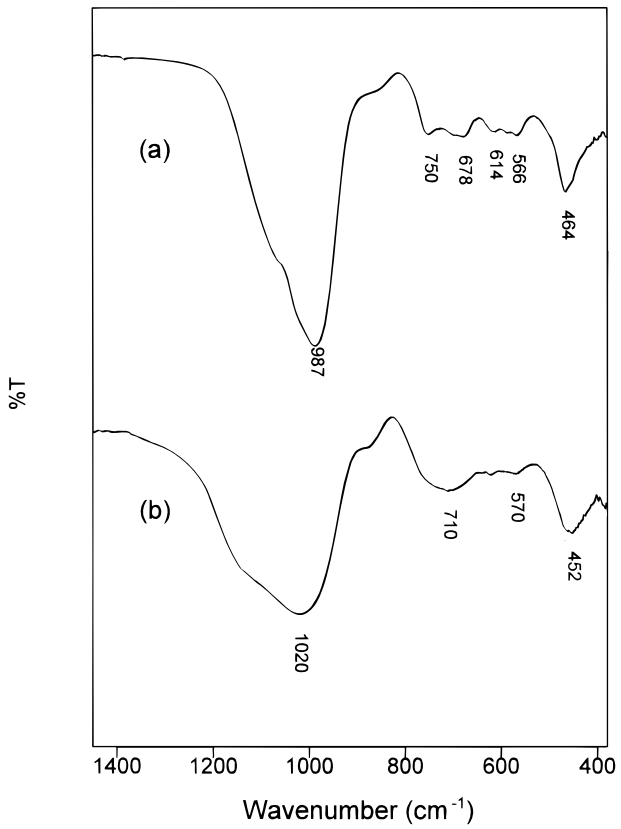

Figure 5. Infrared spectra of (a) as-synthesized zeolite crystals and (b) after synthesis of $Ru(bpy)_3^{2+}-X(10)$.

with 0.1 M NaCl as the final step. Upon comparison to Figures 3a and 4a for the as-synthesized crystals, it is clear that some dealumination of the framework has occurred, as evident from the increase in Si(*n*Al) ($n < 4$) signals as well as Al in octahedral coordination (0 ppm). The infrared spectrum shown in Figure 5b shows a shift of the band at 987 cm^{-1} toward higher frequencies (1020 cm^{-1}) and a decrease in the intensity of the band at 567 cm^{-1}, both features having been reported earlier as characteristic of dealumination.[21] Scanning electron microscopy on the $Ru(bpy)_3^{2+}-$nanocrystalline zeolites showed that the morphology is not altered by the synthesis. The surface area of the crystals prior to complex incorporation was found to be 550 m^2/g. After synthesis, the surface area dropped to 145 m^2/g for $Ru(bpy)_3^{2+}-X(10)$.

To investigate the factors responsible for framework degradation, the as-synthesized Na−X nanocrystals were calcined at 500 °C for 18 h in oxygen and showed a loss in crystallinity of about 45% as estimated from the peak intensities in the diffraction pattern. If the thermal treatment of Na−X was preceded by exposure to mild acidity, the degradation was even more pronounced. Crystallites that were exposed to a pH 5 solution for an hour followed by thermal treatment at 200 °C for 5 h resulted in a material that has only 10% of the intensity of the original sample (treatment similar as in the synthesis of intrazeolitic $Ru(bpy)_3^{2+}$). Figure 4c is the ^{27}Al NMR spectrum of the sample after this treatment. Besides the framework tetrahedral Al signal at 56.4 ppm and the octahedral Al signal at 0 ppm, other signals are observed at 86, 65.2, and 39.6 ppm. The peaks higher than 60 ppm are assigned to $Al(OH)_n^{(3-n)+}$ species and the peak around 40 ppm is assigned to pentacoordinate Al, based on literature reports.[22,23] These signals are not observed in the $Ru(bpy)_3^{2+}-$zeolite X, since washing with NaCl, a step in the purification of $Ru(bpy)_3^{2+}-$zeolite X, removes these species. Previous studies have reported on the disappearance of the five-coordinate Al species on washing.[24] These data suggest that dealumination is occurring upon synthesis of $Ru(bpy)_3^{2+}$. Thus, it is the calcination, the acidic medium for ion-exchange of $Ru(NH_3)_6^{3+}$, and the heat treatment used during the synthesis of $Ru(bpy)_3^{2+}$ that are mainly responsible for the zeolite framework degradation, and a second method was examined to minimize these effects.

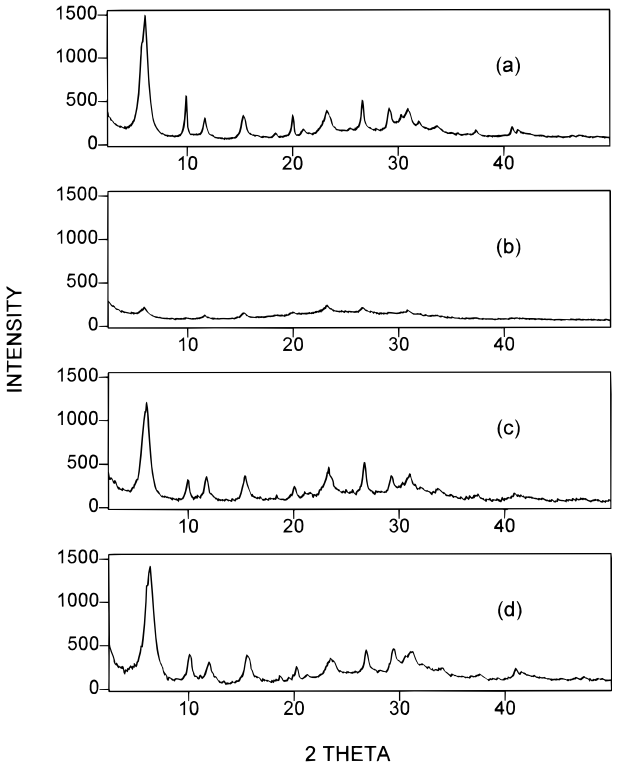

Figure 6. X-ray powder diffraction patterns of (a) as-synthesized crystals, after synthesis of (b) $Ru(bpy)_3^{2+}-X(10)$, (c) $Ru(bpy)_3^{2+}-X(75)$, and (d) $Ru(bpy)_3^{2+}-X(90)$.

Method 2. In the second method, we avoided the calcination step (typically required to oxidize all hydrocarbon impurities in the zeolite) and acidification at pH 5 (usually necessary to avoid formation of ruthenium red). Instead, the Ru red formation was avoided by keeping the temperature low during ion exchange in an anaerobic environment. With this procedure, zeolite degradation was reduced, with a retention of crystallinity of about 75% and a surface area of 370 m^2/g (henceforth referred to as $Ru(bpy)_3^{2+}-X(75)$). Figure 6c shows the diffraction pattern for this sample.

Method 3. On the basis of the degradation observed by method 2, we reasoned that the acidity generated during the formation of $Ru(bpy)_3^{2+}$ from the $Ru(NH_3)_6^{3+}$ species is responsible for this effect. Two reactions have been proposed in the formation of intrazeolitic $Ru(bpy)_3^{2+}$, both of which generate protons:[10a]

$$2Ru(NH_3)_6^{3+} + 6bpy \xrightarrow{200\ °C} 2Ru(bpy)_3^{2+} + N_2H_4 + 10NH_3 + 2H^+$$

$$6Ru(NH_3)_6^{3+} + 18bpy \xrightarrow{200\ °C} 6Ru(bpy)_3^{2+} + N_2 + 34NH_3 + 6H^+$$

Thus, it is clear that, in order to avoid the formation of protons, we need to avoid the reduction step of Ru^{3+}. We synthesized $Ru(bpy)_3^{2+}$ into zeolite X using $Ru(NH_3)_6^{2+}$ as the

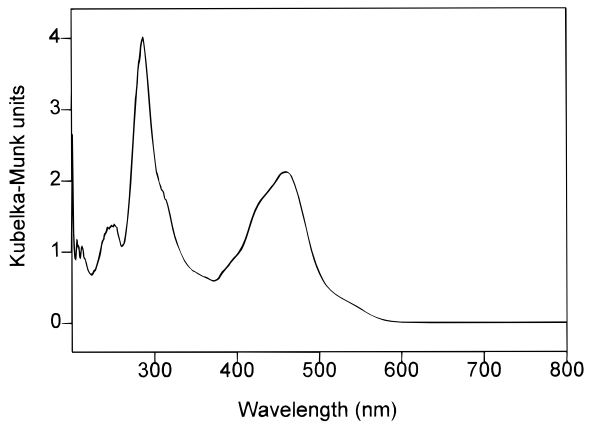

Figure 7. Diffuse reflectance spectrum of $Ru(bpy)_3^{2+}-X(90)$.

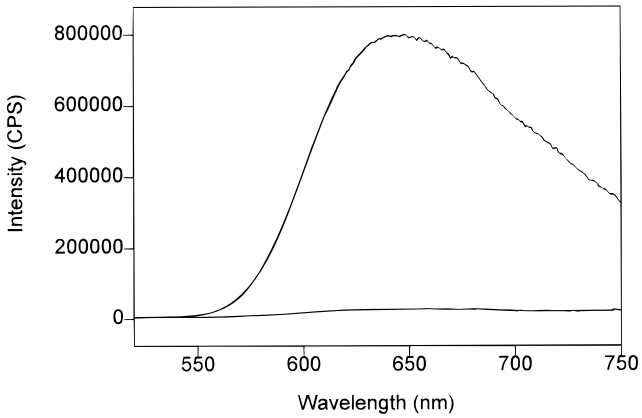

Figure 8. Fluorescence of $Ru(bpy)_3^{2+}-X(90)$ (top) and after exchange with methyl viologen (bottom).

starting material. The difficulty with this procedure is that the $Ru(NH_3)_6^{2+}$ is highly air-sensitive, and the ion-exchange and bpy incorporation procedure needs to be done under anaerobic conditions. This was accomplished, and Figure 7 shows the diffuse reflectance spectrum and Figure 6d the powder diffraction pattern. The electronic spectrum is comparable to earlier published literature by method 1, and the diffraction intensity shows retention of 90% crystallinity and a surface area of 456 m^2/g. The loss of 10% crystallinity was found to arise from the heat treatment during $Ru(bpy)_3^{2+}$ synthesis and therefore represents the best that can be done with the present procedure for these nanocrystallites. We refer to this sample as $Ru(bpy)_3^{2+}-X(90)$.

C. Ion-Exchange and Fluorescence Quenching Properties. We examined the ion-exchange properties of the nanocrystalline zeolite with viologen (bipyridinium cations) molecules. The loadings of *N*,*N*′-methyl-4,4′-bipyridinium (MV^{2+}) in $Ru(bpy)_3^{2+}-X(10)$, $Ru(bpy)_3^{2+}-X(75)$, and $Ru(bpy)_3^{2+}-X(90)$ were 197, 326, and 383 μmol per gram, respectively.

Quenching of the photoexcited $Ru(bpy)_3^{2+}$ by MV^{2+} was also examined. We chose to work with methyl viologen (MV^{2+}) cations, because of significant previous work on intrazeolitic quenching of the $Ru(bpy)_3^{2+}-MV^{2+}$ system.[20,25] The decrease in fluorescence intensity at 610 nm was found to be 85%, 94%, and 97% for $Ru(bpy)_3^{2+}-X(10)$, $Ru(bpy)_3^{2+}-X(75)$, and $Ru(bpy)_3^{2+}-X(90)$, respectively, after ion exchange with MV^{2+}. The data for $Ru(bpy)_3^{2+}-X(90)$ are shown in Figure 8.

Both the lower loading level of viologen and the quenching in degraded crystallites are related and could be a consequence of several factors. First, dealumination decreases the number of ion-exchangeable sites. Second, the presence of extraframework Al formed by dealumination may be filling up the pores. Third, because of framework degradation, there may be pore collapse around the $Ru(bpy)_3^{2+}$ structure, thereby limiting the approach of MV^{2+} molecules ($13.6 \times 6.4 \times 3.8$ Å)[26] into the neighboring sites.

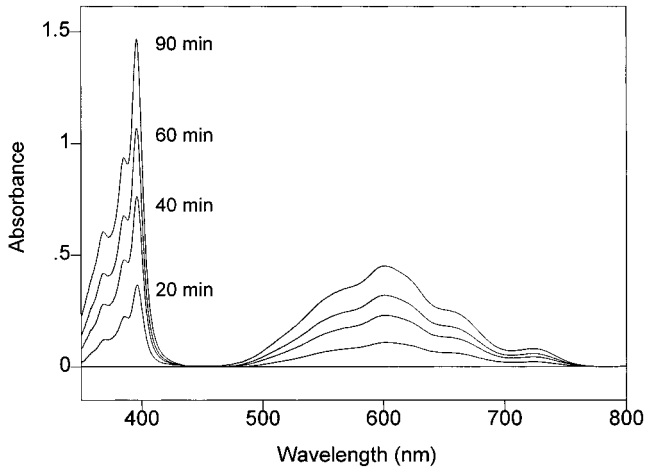

Figure 9. Measure of the growth of $PVS^{\bullet-}$ upon visible photolysis of $Ru(bpy)_3^{2+}-X(90)$ ion-exchanged with DQ^{2+} (spectra taken every 20 min).

D. Charge Separation Efficiencies. Photochemistry using the $Ru(bpy)_3^{2+}-$nanocrystalline zeolites was examined. The system included $Ru(bpy)_3^{2+}-$zeolite with the ion-exchanged viologen *N*,*N*′-tetramethylene-2,2′-bipyridinium dibromide (DQ^{2+}) surrounded by a neutral propyl viologen sulfonate (PVS) in solution. Charges that migrate onto the zeolite surface can be transferred to PVS in the surrounding solution, resulting in permanent charge separation:[27,28]

$$\{Ru(bpy)_3^{2+}\cdots DQ^{2+}\}_z \xrightarrow{h\nu} \{Ru(bpy)_3^{2+*}\cdots DQ^{2+}\}_z$$

$$\{Ru(bpy)_3^{2+*}\cdots DQ^{2+}\}_z \xrightarrow{k_f} \{Ru(bpy)_3^{3+}\cdots DQ^{\bullet+}\}_z$$

$$\{Ru(bpy)_3^{3+}\cdots DQ^{\bullet+}\}_z \xrightarrow{k_b} \{Ru(bpy)_3^{2+}\cdots DQ^{2+}\}_z$$

$$\{Ru(bpy)_3^{3+}\cdots DQ^{\bullet+}\}_z + PVS_s \xrightarrow{k_s} \{Ru(bpy)_3^{3+}\cdots DQ^{2+}\}_z + PVS_s^{\bullet-}$$

where z represents the zeolite and s the solution. Measurement of the reduced viologen ($PVS^{\bullet-}$) in solution by UV−vis spectroscopy provides a good measure of the charge separation efficiency.

Figure 9 shows the results of a typical photolysis experiment for $Ru(bpy)_3^{2+}-X(90)$, which shows the growth of $PVS^{\bullet-}$ radical (390, 620 nm) in solution as a function of photolysis time of the zeolite samples. The rates of radical generation are compared in Figure 10a between $Ru(bpy)_3^{2+}-X(10)$, $Ru(bpy)_3^{2+}-X(75)$, and $Ru(bpy)_3^{2+}-X(90)$ crystallites, along with a "blank" sample, consisting of $Ru(bpy)_3^{2+}-X(90)$ without any ion-exchanged viologen (DQ^{2+}). It is clear that as the crystallinity is preserved, the efficiency of the charge separation process (as measured by the slope of the viologen radical signal versus time) increases. This is probably not surprising, considering that earlier studies on the $Ru(bpy)_3^{2+}-MV^{2+}-$zeolite Y system reported that the charge separation as monitored by the amount of the intrazeolitic viologen radical depended quite critically on the viologen loading.[20] Not only do the viologen molecules have to surround the $Ru(bpy)_3^{2+}$ in order for oxidative quenching to take place, but the packing of viologens per

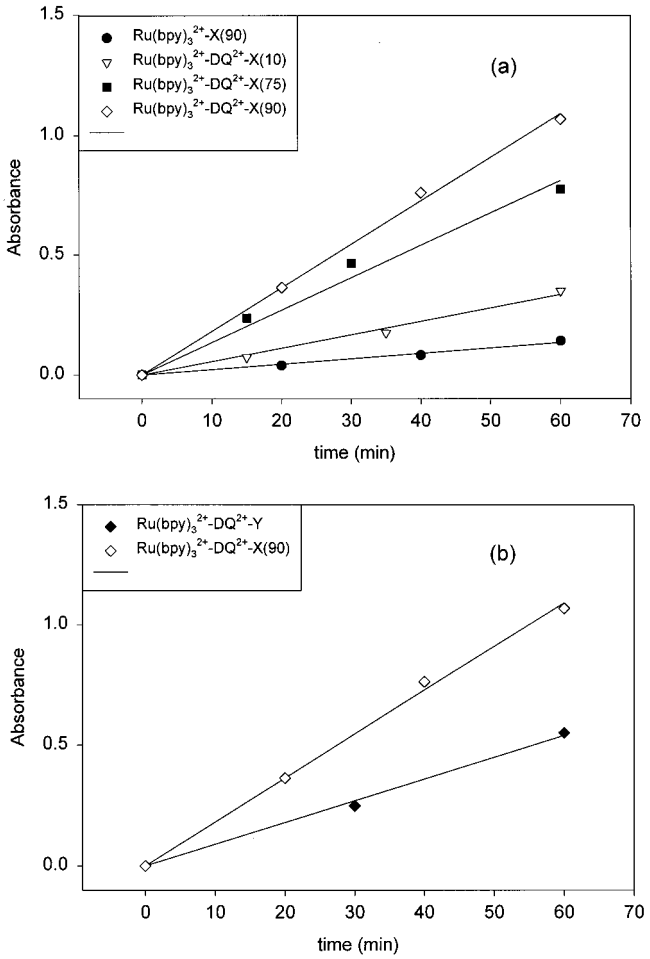

Figure 10. (a) Comparison of the growth of $PVS^{\bullet-}$ during photolysis of $Ru(bpy)_3^{2+}-DQ^{2+}-X(90)$, $Ru(bpy)_3^{2+}-DQ^{2+}-X(75)$, $Ru(bpy)_3^{2+}-DQ^{2+}-X(10)$, and $Ru(bpy)_3^{2+}-X(90)$. (b) Comparison of the growth of $PVS^{\bullet-}$ as a function of time for $Ru(bpy)_3^{2+}-DQ^{2+}-X(90)$ and $Ru(bpy)_3^{2+}-DQ^{2+}-$commercial zeolite Y.

supercage is critical for charge separation to occur. It was proposed that hopping of electrons onto neighboring viologens is necessary to compete with back electron transfer. We interpret the increase in yields of charge separation with framework stability as arising from the ability of the viologen molecules to pack efficiently, thereby increasing the probability of charge transfer by electron hopping via closely spaced viologens to the zeolite surface, from where electron transfer to PVS in solution can occur. The ability of the present photochemical architecture to move charge from within the zeolite to the surface by electron hopping is also evidenced by the improvement of a factor of 8 in charge separation efficiency for $Ru(bpy)_3^{2+}-X(90)$ with and without intrazeolitic DQ^{2+}.

Considering that the charge transfer from the zeolite to the PVS in solution is taking place at the zeolite−solution interface, nanocrystallites should result in higher photochemical yields as compared to regular micron-sized crystallites, based on the higher surface-to-volume ratios. However, because of the extensive aggregation we find in nanocrystalline zeolites, the full advantage of the reduction in crystallite size could not be achieved. Comparison of surface-to-volume ratios for 250 nm aggregates with the 1 μm crystals suggests that a 4-fold improvement is expected. Figure 9c compares the photochemical yields between $Ru(bpy)_3^{2+}-X(90)$ and conventional micron-sized $Ru(bpy)_3^{2+}-$zeolite Y crystallites, the former showing a factor of 2 improvement. There are several factors that can cause the difference between the observed and expected values. First, the scattering properties of the crystallites in the two size ranges are different, and therefore the fraction of light absorbed by the sensitizer can be different. Ideally, we should measure the quantum yield, but this is difficult to determine for these highly scattering samples. Second, there is a broad distribution of sizes in both the zeolite X and Y samples, although the former is definitely smaller. Third, the ion-exchange capacity of the $Ru(bpy)_3^{2+}-X(90)$ toward viologens is almost a factor of 2 lower than the conventional zeolite Y crystallites,[20,25,29] reasons for which are unclear at the present.

However, it is clear from this study that if well-dispersed $Ru(bpy)_3^{2+}$-containing nanocrystallites can be synthesized, then use of the sensitizer-donor strategy described in this paper will lead to significant improvements in photochemical charge separation. This is currently being pursued.

Conclusions

Small (13 nm) zeolite X crystallites forming aggregates of 250 nm was synthesized by using a low-temperature aging process in the presence of sucrose. Conventional ship-in-a-bottle synthesis of $Ru(bpy)_3^{2+}$ in these zeolites leads to extensive framework degradation, with only 10% of the diffraction intensity remaining as compared to the original samples. It was discovered that the structural collapse occurred due to exposure to slightly acidic conditions (pH 5) and thermal treatment, necessary for synthesis of $Ru(bpy)_3^{2+}$. When the procedure was modified to remove the exposure to acidity, about 75% of the crystallinity could be preserved. During synthesis of $Ru(bpy)_3^{2+}$ from $Ru(NH_3)_6^{3+}$, acidity is generated. The synthesis was further modified to begin with $Ru(NH_3)_6^{2+}$, and it was found that $Ru(bpy)_3^{2+}-$zeolite retaining 90% of the crystallinity could be made. The loss of 10% crystallinity arises from the thermal treatment during $Ru(bpy)_3^{2+}$ synthesis and could not be avoided. Ion exchange and fluorescence quenching of $Ru(bpy)_3^{2+}-$zeolite by viologens showed an increase as the zeolite crystallinity is preserved. Photolysis of $Ru(bpy)_3^{2+}-$viologen−zeolite in the presence of neutral propyl viologen sulfonate in solution also showed an increase in permanent charge separation efficiency as the crystallinity of the $Ru(bpy)_3^{2+}-$zeolite increased. Because of increased surface-to-volume ratio of the nanocrystallites as compared to conventional micron-sized zeolite Y, photochemical charge separation efficiency was found to be a factor of 2 better with the small crystallites. It is important to stress that this improvement arises from the smaller crystallite size and provides a rationale for synthesizing well-dispersed nanocrystallites.

Acknowledgment. We gratefully acknowledge the support of DOE, Basic Energy Sciences, for funding this research. We are thankful to Dr. Michael Ledney for initiating this research program. Helpful discussions with Dr. Charles Kresge are also acknowledged.

References and Notes

(1) (a) Charnell, J. F. *J. Cryst. Growth* **1971**, *8*, 291. (b) Kuperman, A.; Nadimi, S.; Oliver, S.; Ozin, G. M.; Garces, J. M.; Olken, M. M. *Nature* **1993**, *365*, 239.

(2) Auroux, A.; Huang, M.; Kaliaguine, S. *Langmuir* **1996**, *12*, 4803.

(3) (a) Persson, A. E.; Schoeman, B. J.; Sterte, J.; Otterstedt, J. E. *Zeolites* **1995**, *15*, 611. (b) Lovallo, M. C.; Tsapatasis, M. In *Advanced Catalysts and Structured Materials*; Moser, W. R., Ed.; Academic Press: San Diego, 1996; p 307.

(4) (a) Yamamura, M.; Chaki, K.; Wakatsuki, T.; Okado, H.; Fujimoto, K. *Zeolites* **1994**, *14*, 643. (b) Sterte, J.; Mintova, S.; Zhang, G.; Schoeman, B. J. *Zeolites* **1997**, *18*, 387.

(5) (a) Bedioui, F.; Devynck, J.; Balkus, K. J. *J. Phys. Chem.* **1996**, *100*, 8607. (b) Rolison, D. R.; Bessel, C. A.; Baker, M. D.; Senaratne, C.; Zhang, J. *J. Phys. Chem.* **1996**, *100*, 8610.

(6) Hoelderich, W. F.; Hesse, M.; Naumann, F. *Angew. Chem., Int. Ed. Engl*. **1988**, *27*, 226

(7) Ledney, M.; Dutta, P. K. *Prog. Inorg. Chem.* **1997**, *44*, 2209.

(8) (a) Schoeman, B. J.; Sterte, J.; Otterstedt, J. E. *Zeolites* **1994,** *14*, 110. (b) Otterstedt, J. E.; Sterte, J.; Schoeman, B. J. International Patent, WO 94/05597, 1994.

(9) Ambs, W. J. U.S. Patent, 4.372.931, 1983.

(10) (a) Quayle, W. J.; Lunsford, J. H. *Inorg. Chem.* **1982**, *21*, 97. (b) Dutta, P. K.; Incavo, J. A. *J. Phys. Chem.* **1987**, *91*, 4443.

(11) Cullity, B. D. *Elements of X-Ray Diffraction;* Addison-Wesley: Reading, MA, 1978.

(12) (a) Homer, R. F.; Tomlinson, T. E. *J. Chem. Soc.* **1960**, 2498. (b) Degani, T.; Wilner, I. *J. Am. Chem. Soc.* **1983**, *105*, 6228.

(13) Manley-Harris, M.; Moody, W.; Richards, G. N. *Aust. J. Chem.* **1980**, *33*, 1041.

(14) Martin, R. B. *Clin. Chem.* **1986**, *32*, 1797.

(15) Sand, L. B.; Sacco, A.; Thompson, R. W.; Dixon, A. G. *Zeolites* **1987**, *7*, 387.

(16) (a) Ramdas, S.; Thomas, J. M.; Klinowski, J.; Fyfe, C. A.; Hartman, J. S. *Nature* **1981**, *292*, 228. (b) Engelhardt, G.; Lippmaa, E.; Mägi, M. *J. Chem. Soc., Chem. Commun.* **1981**, 712.

(17) Flanigen, E. M.; Khatami, H. J.; Szymanski, H. A. In *Molecular Sieve Zeolites−1I;* Adv. Chem. Ser. 101; American Chemical Society: Washington, DC, 1971; p 201.

(18) (a) Angell, C. L. *J. Phys. Chem.* **1973**, *77*, 22. (b) Dutta, P. K.; Shieh, D. C.; Puri, M. *Zeolites* **1988**, *8*, 306.

(19) (a) Tiong, K. K.; Amritharaj, P. M.; Pollak, F. H.; Aspner, D. E. *Appl. Phys. Lett.* **1984**, *44*, 122. (b) Richter, H.; Wang, Z. P.; Ley, L. *Solid State Commun.* **1981**, *39*, 625. (c) Graham, G. W.; Weber, W. H.; Peters, C. R.; Usmen, R. *J. Catal.* **1991**, *130*, 310.

(20) Dutta, P. K.; Turbeville, W. *J. Phys. Chem.* **1992**, *96*, 9410.

(21) Cairon, O.; Khabtou, S.; Balanzat, E.; Janin, A.; Marzin, M.; Chambellan, A.; Lavalley, J. C.; Chevreau, T. In *Zeolites and Related Microporous Materials: State of the Art 1994*; *Studies in Surface Science and Catalysis;* Weitkamp, J., Karge, H. G., Pfiefer, H., Hölderich, W., Eds.; Elsevier: Amsterdam, 1994; Vol. 84, p 997.

(22) (a) Freude, D.; Haase, J.; Pfiefer, H.; Prager, D.; Sheler, G. *Chem. Phys. Lett.* **1985**, *114*, 143. (b) Samoson, A.; Lippmaa, E.; Engelhardt, G.; Lohse, U.; Jerschkewitc, H.-G. *Chem. Phys. Lett.* **1987**, *134*, 589.

(23) Ray, G. J.; Samoson, A. *Zeolites* **1994**, *13*, 410.

(24) Gilson, J.-P.; Edwards, G. C.; Peters, A. W.; Rajagopalan, K.; Warsmbecher, R. F.; Roberie, T. G.; Shatlock, M. P. *J. Chem. Soc., Chem. Commun.* **1987**, 91.

(25) Kim, Y. I.; Mallouk, T. E. *J. Phys. Chem.* **1992**, *96*, 2879.

(26) Summers, L. A. *The Bipyridinium Herbicides*; Academic Press: New York, 1980.

(27) Borja, M.; Dutta, P. K. *Nature* **1993**, *362*, 43.

(28) Sykora, M.; Kincaid, J. R. *Nature* **1997**, *387*, 162.

(29) Gemborys, H. A.; Shaw, B. R. *J. Electroanal. Chem.* **1986**, *208*, 95.